

# Supplementary Information

## Direct Electrical Junction Formation of Highly Vertical Aligned Zinc Oxide Nanorods

Tae Il Lee, Woo Soon Jang, Ji Hyeon Park, Youn Hee Kang, Sang Hoon Lee, Sung Hwan Hwang, Hong Koo Baik and Jae Min Myoung\*

*Department of Materials Science and Engineering, Yonsei University, Seoul, Korea*

### 1. Monolayer of hexagonal $\beta$ -Co(OH)<sub>2</sub> NPs.

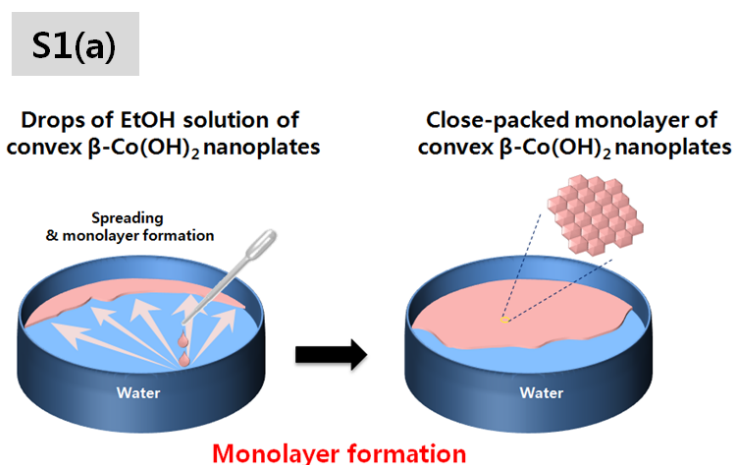


**Figure S1(a)** a process, alcohol dropping on water for self-assembled monolayer of convexo-convex  $\beta$ -Co(OH)<sub>2</sub> NP,

A schematic diagram shown in Figure S1(a) describes how to make two-dimensional (2D) monolayer of hexagonal  $\beta$ -Co(OH)<sub>2</sub> NPs. Mono-dispersed ethanol solution of hexagonal  $\beta$ -

$\text{Co(OH)}_2$  NPs was dropped on water. During these dropping events, a 2D array of the  $\beta\text{-Co(OH)}_2$  NPs was spontaneously formed within a few second. Three sequential steps related to the miscible process of dropping ethanol into the water were employed for the formation of the 2D array: spreading, trapping, and packing. When a droplet of ethanol meets the water, some portion of the ethanol goes into the water and another portion is spread on the surface because there is a kinetic time delay in the miscible process of ethanol and water. The  $\beta\text{-Co(OH)}_2$  NPs in the entering portion are mixed with the water; whereas, those in the spreading portion, as the ethanol is gradually dispersed into the water, are trapped by the net force of the surface tension between the air and water. On the surface area confined by the Petri dish, due to the surface pressure from the ethanol spreading, the trapped  $\beta\text{-Co(OH)}_2$  NPs are stacked two-dimensionally at the opposite side of the wall from the dropping position.

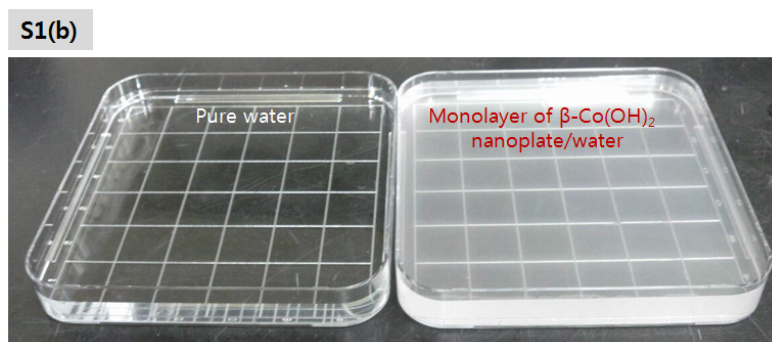


**Figure S1(b).** 15 cm by 15 cm scale monolayer of convexo-convex  $\beta\text{-Co(OH)}_2$  NPs floated on water. Naturally, the color of  $\beta\text{-Co(OH)}_2$  is pink, so Petri-dish contained the monolayer looks like being covered with a thin white-pinky layer.

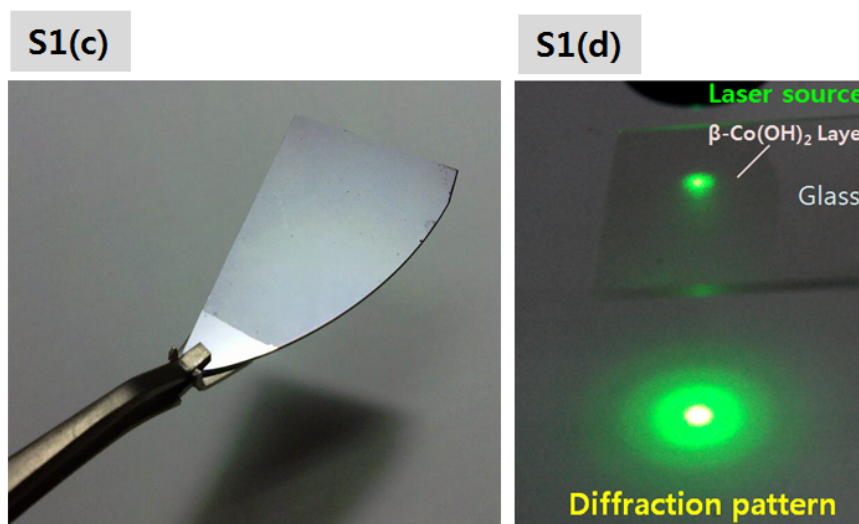


**Figure S1(c-d)** c. Transferred monolayer of convexo-convex  $\beta\text{-Co(OH)}_2$  NP on silicon wafer, d. Ring diffraction pattern of 512 nm laser after transmitting the monolayer deposited on glass.

In this work, up to 15 cm by 15 cm scale, the 2D monolayer of  $\beta\text{-Co(OH)}_2$  NPs was assembled at air/water interface as shown in Figure S1(b) Figure S1(c) shows a transferred uniform 2D monolayer of hexagonal  $\beta\text{-Co(OH)}_2$  NPs on 3 cm by 2 cm silicon wafer. Furthermore, to evaluate the large scale uniformity of the monolayer, a transmitted diffraction

pattern of 512 nm laser source vertically incident into the monolayer on a glass substrate was determined, and as a result, a clear ring pattern was observed as shown in Figure S1(d). The ring pattern represents that the monolayer was composed of close-packed single crystalline hexagonal  $\beta$ -Co(OH)<sub>2</sub> NPs with vertically preferred-orientation over the large area.

## 2. Growth of ZnO NRs on convexo-convex hexagonal $\beta$ -Co(OH)<sub>2</sub> NPs.

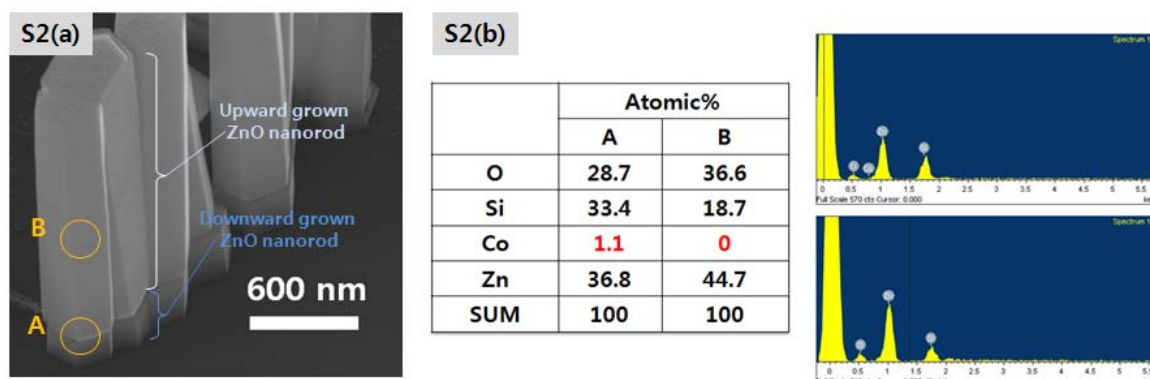


**Figure S2(a-b).** a vertically attached upward and downward grown ZnO NRs with each other on silicon wafer, b. the results of EDX analysis at the surface upward grown ZnO NRs and boundary region of twin-grown ZnO NRs. The atomic percent of cobalt atom were roughly determined at a point A, the interface of these counter currently grown ZnO NRs and point B, the surface of upward grown ZnO NRs. As a result, there is no signal of cobalt component at point B, whereas, it were detected by the level of about 1.1 % at point A.

The quantity of cobalt atom were roughly determined at a point A, the interface of these counter currently grown ZnO NRs and point B, the surface of upward grown ZnO NRs indicated in Figure S2(a). As a result, there is no signal of cobalt component at point B, whereas, it was detected by the level of about 1.1 % at point A (see Figure S2(b)). From the EDX result, it is thought that the dissolved cobalt ions did not take part in the synthesis of ZnO NRs at point B and the weak signal of cobalt atoms at point A comes from the still remained  $\beta$ -Co(OH)<sub>2</sub> in the interface.

## 3. Density control of ZnO NRs

To demonstrate the density controllability of ZnO NRs up to continuous film on convexo-convex  $\beta$ -Co(OH)<sub>2</sub> NPs, the concentration of zinc divalent ions were varied from 70 to 175 mM. Because the radial growth of ZnO NRs is dominant in zinc ion rich condition, at a fixed growth time 12 h, the diameter of ZnO NRs increased to fill the space among the NRs as zinc ion's concentration increased, whereas their heights were similar in all cases as shown in Fig. 3S(a-d). At 175 mM, all ZnO NRs were laterally coarsened with each other, but micro sized pore as the geometrical center of the edge growth on convexo-convex  $\beta$ -Co(OH)<sub>2</sub> NPs were observed as shown in Fig. 3S(d). Furthermore, if a secondary step employing different anions such as chloride and citrate ion to grow radial direction is applied to the vertically grown ZnO

NRs in this work, a (0001) preferred oriented pore-free ZnO film will be obtained.

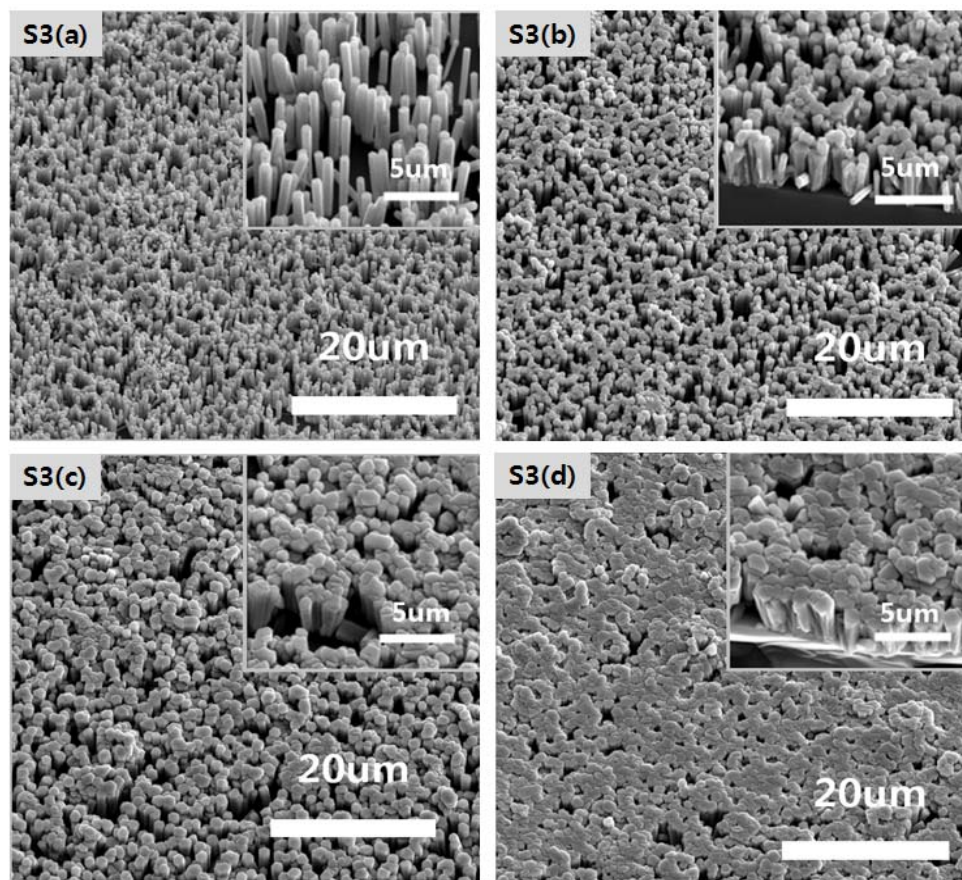


**Figure S3** The density controlled ZnO NRs up to continuous film on convexo-convex  $\beta$ -Co(OH)<sub>2</sub> NPs through the variation of concentration of zinc divalent ions from **a.** 70 mM, **b.** 105 mM **c.** 140 mM **d.** 175 mM.

#### 4. Devices (p-n diode and Schottky diode)

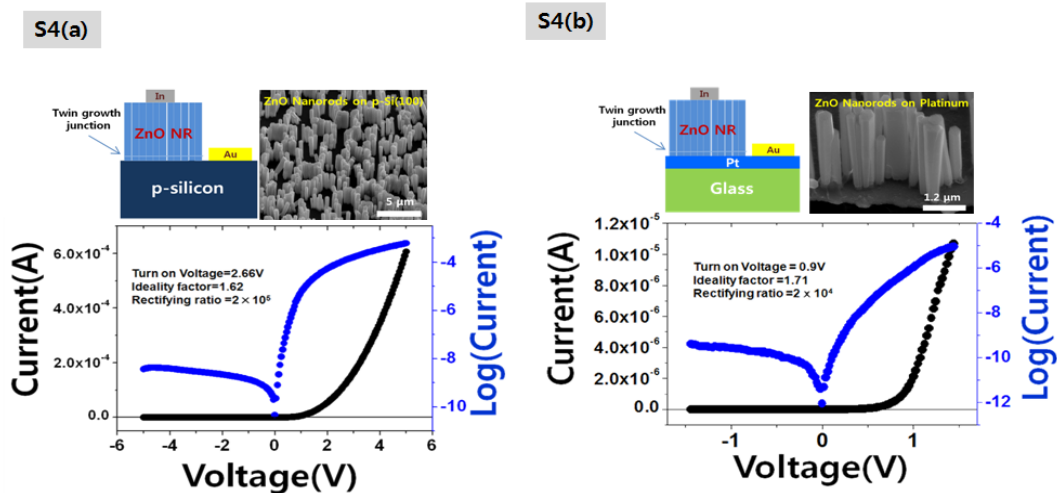


**Figure S4(a-b)** **a.** direct grown ZnO NRs on a p-type silicon wafer and its p-n diode *I-V* characteristics **b.** direct grown ZnO NRs on a platinum layer and its Schottky diode *I-V* characteristics.

Generally, ZnO NRs synthesized using hydrothermal process shows n-type semiconducting property, hence a p-type silicon wafer was adopted to fabricate a p-n junction diode with the ZnO NRs, and its electrical characteristic was exhibited in Fig. S4(a). After 5 h growth of ZnO NRs with a fixed 70 mM at 80 °C, gold and indium electrode were formed as shown in a schematic diagram in Fig. S4(a). Turn-on voltage and rectifying ratio were measured by 2.66 V and  $10^5$  respectively. Using the plot of the  $\ln(\text{current})$  vs.  $\text{voltage}$ , the ideality factor was calculated as 1.66 within the voltage range  $0.1 \text{ V} < V < 0.5 \text{ V}$ .

For Schottky contact device, platinum having a high work function as well as playing a role in passivation to grow ZnO NRs was selected as a proper test vehicle to confirm the ability of the sacrificial template to form Schottky contact with ZnO NRs in this work. A Schottky diode composed of ZnO NRs and platinum was fabricated, and the electrical characteristic of this device was exhibited in Fig. S4(b). After 5 h growth of ZnO NRs with a fixed 70 mM at 80 °C, gold and indium electrode were deposited as shown in a schematic diagram in Fig. S4(b). As shown in SEM image of Fig. S4(b), vertically well aligned ZnO NRs grown on a platinum layer were clearly observed. Turn-on voltage and rectifying ratio were measured by 0.9 V and  $10^4$  respectively. Using the plot of the  $\ln(\text{current})$  vs.  $\text{voltage}$ , the ideality factor was calculated as 1.71 within the voltage range  $0.02 \text{ V} < V < 0.4 \text{ V}$ . Despite of low temperature solution process, through our sacrificial template, ZnO NRs based p-n and Schottky diodes fabricated with p-type silicon wafer and platinum film respectively showed considerable electrical performances in comparison with vacuum processed cases <sup>1,2</sup>.

## 5. Methods

**Synthesis of  $\beta$ -Co(OH)<sub>2</sub> nanopalte:** Hexagonal  $\beta$ -Co(OH)<sub>2</sub> NPs were synthesized by the precipitation of an aqueous solution of cobalt(II) chloride hexahydrate through the hydrolysis assisted by hexamethylenetetramine (HMTA) in the 200 ml mixing solvent, water/ethanol (9:1, v/v). The synthesis was executed at a fixed mole fraction of divalent cobalt and HMTA (1:1), temperature (90 °C) and concentration (5 mM) for 45 min. As-synthesized  $\beta$ -Co(OH)<sub>2</sub> NPs were purified using three-times centrifugation at 4000 rpm and were then dispersed in 99.99 % ethanol.

**Material characterization of  $\beta$ -Co(OH)<sub>2</sub> nanopalte and ZnO nanorods:** X-ray diffraction pattern of 2D assembled monolayer of  $\beta$ -Co(OH)<sub>2</sub> nanopalte was obtained using a XRD (Model Ultima IV). The surface shape of  $\beta$ -Co(OH)<sub>2</sub> nanopalte was measured using a AFM (Asylum, Model MFP-3D-SA). EDX analysis of ZnO NRs was executed using SEM (JEOL, JSM-7001F). The 45° tilted view of  $\beta$ -Co(OH)<sub>2</sub> nanopalte and ZnO nanorods was characterized by using SEM (JEOL, JSM-7001F).

**Growth of ZnO NRs on  $\beta$ -Co(OH)<sub>2</sub> nanopalt and real time pH tendency measurement:** ZnO NRs were grown by the precipitation of an aqueous solution of zinc(II) nitrate hexahydrate through the hydrolysis assisted by HMTA in the 20 ml bial bottle. The synthesis was executed at a fixed mole fraction of divalent cobalt and HMTA (1:1), temperature (80 °C) at a certain concentration for various times. As-grown ZnO NRs were washed using DI water and ethanol by several times, and then dried for 12 h at 60 °C. The temporal pH tendency

was determined using a digital pH meter (Hanna, Model HI 4222) at a fixed mole fraction of divalent zinc and HMTA (1:1), temperature (80°C) and concentration (70 mM) for 60 min.

**I-V characterization:** Current-voltage (I-V) data were measured by using an Agilent semiconductor parameter analyzer (Model 4145B), with contacts to the devices made by using a probe station (Desert Cryogenics, Model TTP4).

## 6. Reference

- 1 S. T. Tan, X. W. Sun, J. L. Zhao, S. Iwan, Z. H. Cen, T. P. Chen, J. D. Ye, G.Q. Lo, D. L. Kwong and K. L. Teo, *Appl. Phys. Lett.* 2008, **93**, 013506.
- 2 Y. Z. Li, X. M. Li, C. Yang, X. D. Gao and Y. J. He, *Phys. D: Appl. Phys.* 2010, **43**, 285101.